Islam, Md Towhidul, Parsons, Andrew J, Nuzulia, Nur Aisyah, Sari, Yessie W., Ren, Hong, Booth, Jonathan and Ahmed, Ifty (2023) *Process parameter optimisation for manufacturing porous bioactive silicate glass microspheres via flame spheroidisation: The goldilocks effect.* Journal of Non-Crystalline Solids, 614 . ISSN 0022-3093.

Process parameter optimisation for manufacturing porous bioactive silicate glass microspheres via flame spheroidisation: The goldilocks effect

Md Towhidul Islam [a,b,c], Andrew J Parsons [d], Nur Aisyah Nuzulia [e], Yessie W. Sari [e], Hong Ren [f], Jonathan Booth [f], Ifty Ahmed [a,*]

[a] *Advanced Materials Research Group, Faculty of Engineering, University of Nottingham, Nottingham, NG7 2RD, United Kingdom*
[b] *Department of Applied Chemistry and Chemical Engineering, Faculty of Engineering, Noakhali Science and Technology University, Noakhali 3814, Bangladesh*
[c] *School of Physical Sciences, University of Kent, Canterbury CT2 7NZ, United Kingdom*
[d] *Composites Research Group, Faculty of Engineering, University of Nottingham, Nottingham NG7 2RD, United Kingdom*
[e] *Department of Physics, Faculty of Mathematics and Natural Sciences, Bogor Agricultural University Kampus IPB Darmaga, Darmaga-Bogor 16680, Indonesia*
[f] *Johnson Matthey, Blounts Court, Sonning Common, Reading RG4 9NH, United Kingdom*

ABSTRACT

This study investigated the influence of flame spheroidisation process parameters for successfully manufacturing solid (dense) and highly porous microspheres from Food and Drug Administration approved bioactive 45S5 glass and 45S5 with addition of viscosity modifiers (i.e. 2 and 5 mol% borax and V_2O_5), compared against successfully processed phosphate glass microspheres (termed P40). Characterisation studies performed included thermal analysis (SDT), glass viscosity measurements using high temperature rotational viscometry and hot stage microscopy, X-ray diffraction, scanning electron microscopy and energy dispersive X-ray analysis.

This study revealed that aside from intrinsic material properties (i.e. melt temperature and viscosity profiles), process parameters including starting glass particle size, cooling rate and gas flow rates were important factors in achieving the desired porous glass microsphere morphology. Considering the above influential factors, a processing model has been proposed for the manufacture of highly porous microspheres from bioactive silicate glasses.

1. Introduction

Bioactive glasses have been hugely successful in the field of biomedical applications and especially for hard tissue repair applications. Creating the ability to tailor their morphologies would not only strongly influence their future applicability but would also enable a wider range of applications. In particular, glass particles with spherical morphology provide the advantage of uniformity in size and shape, and can be delivered to target tissues via minimally invasive injection procedures [1,2]. Spherical morphologies can also provide enhanced versatility in filling defect shapes compared to bulk scaffolds which tend to have pre-set shapes [3]. Moreover, the addition of porosity further increases the surface area and if the external pores can be made large enough, this would allow for efficient cell attachment, encapsulation and proliferation which could be exploited to deliver varying payloads (such as cells, drugs, growth factors or other biologics). Also, creating interconnected porosity throughout each of the microspheres would

enable the flow of oxygen and nutrient by-products [4]. The pore sizes are also important factors to determine the adsorption and release of biomolecules and can also influence blood vessel formation and bone in-growth [5]. Several studies have been conducted to define the influence of material pore size on the outcome of new bone formation *in vivo*, with contrasting results. For instance, when comparing ceramic scaffolds with pore sizes ranging between 50 and 500 μm, larger pores were associated with more bone formation [6–8]. However, opposing outcomes have been reported by Diao *et al.*, where it was observed that 100 μm pore sized scaffolds performed better than 250 and 400 μm pore sized scaffolds [9].

Microspheres can be prepared using various processing methods such as sol-gel, tube furnace method and flame spheroidisation, as examples [10]. From these, flame spheroidisation is a relatively rapid and inexpensive process, and can easily be scaled-up for commercialisation purposes. However, there are several parameters of the flame spheroidisation process which can influence the desired outcome of sphere

Table 1
Compositions of eight different glasses investigated.

Glass Formulation	SiO$_2$ (mol%)	P$_2$O$_5$ (mol%)	CaO (mol%)	Na$_2$O (mol%)	MgO (mol%)	K$_2$O (mol%)	Borax (Na$_2$B$_4$O$_7\cdot$10H$_2$O)	V$_2$O$_5$
45S5	46.1	2.6	26.9	24.4	0	0	0	0
S53P4	53.8	1.7	21.8	22.7	0	0	0	0
13–93	54.6	1.7	22.1	6	7.7	7.9	0	0
45S5 + 2 mol% Borax	46.1	2.6	26.9	22.4	0	0	2	0
45S5 + 5 mol% Borax	46.1	2.6	26.9	19.4	0	0	5	0
45S5 + 2 mol% V$_2$O$_5$	46.1	2.6	26.9	22.4	0	0	0	2
45S5 + 5 mol% V$_2$O$_5$	46.1	2.6	26.9	19.4	0	0	0	5
P40	0	40	16	20	24	0	0	0

size and shape. For example, i) particle separation prior to entering the flame is a key criterion to obtain dispersed uniform spheres; ii) particle residence time in the flame is also an important factor as larger particles (or high melt-temperature materials) may require longer residence times to sufficiently melt, iii) the flame temperature can also influence outcomes of the microspheres produced and is generally controlled by the type of fuel and ratios used [11]. Several studies have utilised varying gases to create a flame including oxygen/propane, oxygen/acetylene, oxygen/petrol [12] and natural gas/air flames [11,13,14].

The initial development of manufacturing porous phosphate-based glass (PBG) microspheres started within the Advanced Materials Research Group (AMRG) at the University of Nottingham (UoN), with attempts to make these materials porous so that they could be exploited for delivery and release of varying biological payloads. Hossain *et al.* prepared highly porous and fully interconnected PBG microspheres (P40; 40P$_2$O$_5\cdot$16CaO$\cdot$24MgO$\cdot$20Na$_2$O in mol%) via the flame spheroidisation process [2]. The same manufacturing process was also recently applied to produce highly porous borate glass microspheres which were subsequently converted into porous hydroxyapatite microspheres [15].

There are only a few studies which report on the development of porous microspheres from melt-derived silicate-based materials [16–18]. The preparation of porous silicate-based glass (45S5) microspheres via flame synthesis was undertaken by Kraxner *et al.* [18]. However, their process resulted in porous microspheres which were not fully amorphous as a sodium calcium silicate crystalline phase was observed [18]. Moreover, their process resulted in a markedly different formulation when compared to the starting 45S5 glass powder with 11 wt% higher SiO$_2$ content for the porous microspheres [18]. Furthermore, no information on the yield of porous microspheres was reported.

The aim of this study was to explore the manufacturing of bioactive silicate glasses (i.e. 45S5) into highly porous microspheres using the flame spheroidisation process developed in our group. The key objective of this study was to investigate the effect of process parameters on manufacture of highly porous microspheres. The characterisation studies for the materials were performed via thermal analysis (simultaneous thermal analysis instrument, SDT), viscosity measurements, using high temperature rotational viscometer (HTV) and hot stage microscopy (HSM), scanning electron microscopy (SEM) and energy dispersive X-ray (EDX) and X-ray diffraction analysis.

2. Materials and methodology

2.1. Glass preparation

In this study seven bioactive silicate glass formulations (including P40 phosphate-based glass for comparison) were prepared using sodium carbonate (Na$_2$CO$_3$), potassium carbonate (K$_2$CO$_3$), calcium carbonate (CaCO$_3$), magnesium carbonate (Mg$_2$CO$_3$), sodium dihydrogen phosphate (NaH$_2$PO$_4$), calcium hydrogen phosphate (CaHPO$_4$), magnesium hydrogen phosphate trihydrate (MgHPO$_4\cdot$3H$_2$O), phosphorous pentoxide (P$_2$O$_5$), silicon dioxide (SiO$_2$), borax (Na$_2$B$_4$O$_7\cdot$10H$_2$O) and V$_2$O$_5$ as starting materials (Sigma Aldrich, UK $\geq$ 99%). The composition of glasses produced is shown in Table 1. The required amounts of

precursors for silicate-based glasses were weighed, mixed and transferred to a platinum rhodium alloy crucible (Birmingham Metal Company, U.K.) which was then placed into a furnace and followed a controlled program using 10 °C /min ramp for melting (at 350 °C for 0.5 h to remove H$_2$O, at 800 °C for 0.5 h to remove CO$_2$ and at 1380 °C for 2 h for melting). The mixture of precursors for phosphate-based glass was pre-heated at 350 °C for 0.5 h to remove H$_2$O and then melted at 1150 ºC for 1.5 h. The resulting molten glass was poured onto a steel plate and left to cool to room temperature.

2.2. Preparation of porous silicate and phosphate-based glass microspheres

Glass particles from silicate and phosphate formulations in the size range of 63–125 μm (obtained after grinding the glasses in ball mill and sieving the particles) were mixed with a porogen (calcium carbonate or strontium carbonate) with 1:3 ratio of glass particles to porogen and then processed via flame spheroidisation to prepare porous glass microspheres (PGMS), as described elsewhere [2]. Porous phosphate glass microspheres were then washed using acetic acid (5 M) for 2 mins followed by a wash-step using deionised water for 5 mins and then dried at 50 °C overnight [2]. For the porous silicate glass microspheres, the wash-step involved using 0.5 M acetic for 1 min, followed by post-washing using deionised water, which were also dried at 50 °C overnight [19].

3. Characterisation methods

3.1. Scanning electron microscopy (SEM) and energy dispersive X-ray (EDX) analysis

Scanning electron microscopy (SEM- Philips XL30, FEI, USA) with accelerating voltage of 15 kV and a working distance of 10 mm, was used to determine the morphology of the microspheres. The microspheres were fixed onto aluminium stubs with conductive carbon sticky tabs and sputter coated (Agar Sputter Coater) with platinum prior to examination. Compositional analysis for the glass particles/microspheres were carried out using EDX analysis by embedding the particles/microspheres in a cold set epoxy resin and polishing with SiC paper followed by a diamond cloth and then coating with carbon using an evaporation coater (Edwards coating System E306A). EDX analysis was performed on both area and 5 separate spots on each sample and an average value was taken.

3.2. X-ray diffraction analysis

X-ray diffraction analysis was used to explore the amorphous nature of each glass formulation both as particulates and as porous microspheres, using a Bruker D8 Advanced diffractometer (BRUKER AXS, Germany). The instrument was operated at room temperature and ambient atmosphere with Ni-filtered CuKα radiation (λ=0.15418 nm), generated at 40 kV and 35 mA. Data were collected from 8° to 50° 2θ diffraction angle using a scan step time of 8 s and step size of 0.04°. Phases were identified using the EVA software (DIFFRACplus suite,
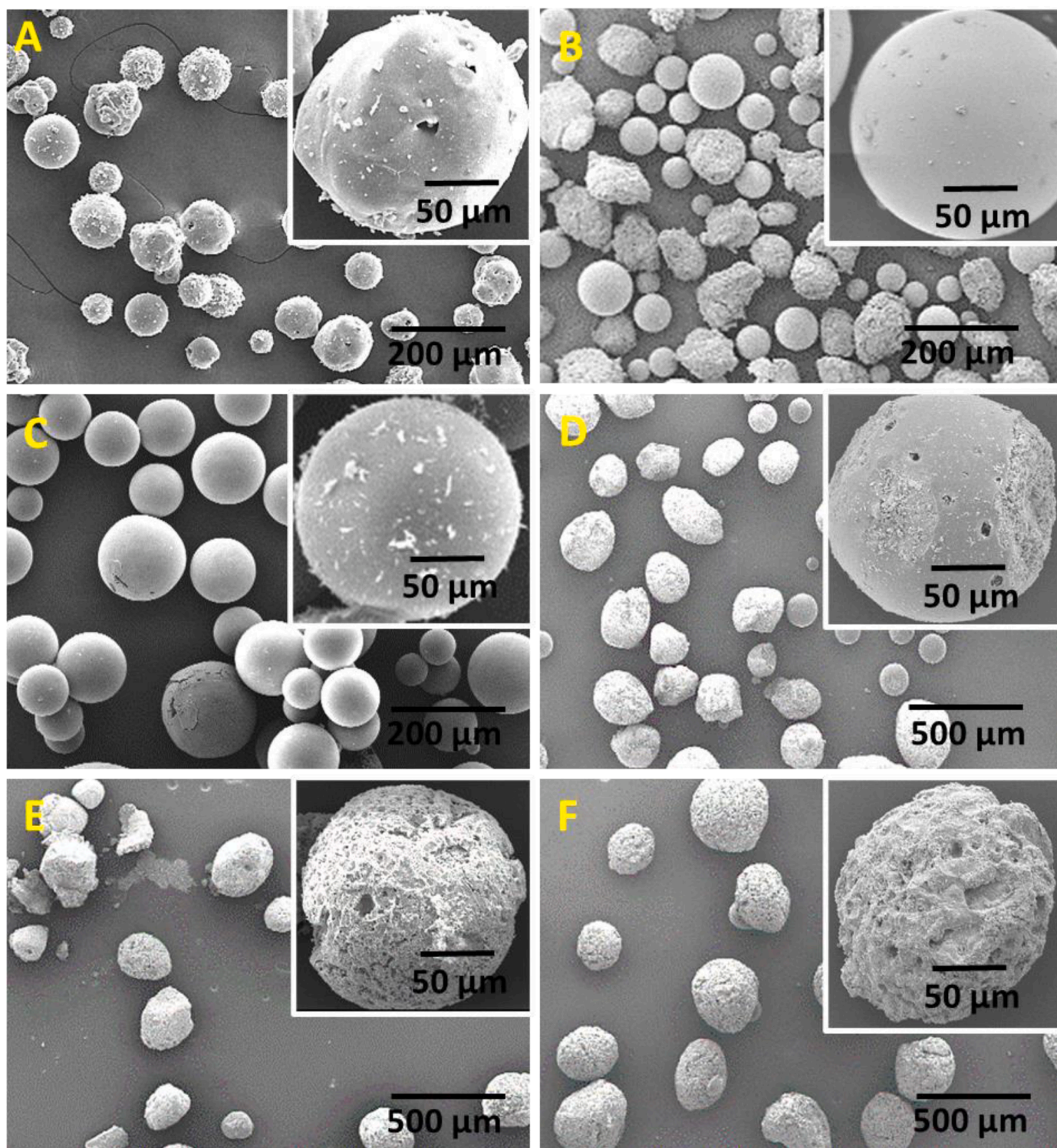
Fig. 1. Initial attempts to prepare porous A) 45S5, B) S53P4 and C) 13–93 bio-silicate glass microspheres using $CaCO_3$ porogen via conventional method. Trials exploring D) particles: $SrCO_3$ (1:3), E) particles: $SrCO_3$ (1:4) and F) particles: $SrCO_3$ (1:5) to improve the yield and porosity for 13–93 bio-silicate glass microspheres.

Bruker-AXS) and the International Centre for Diffraction Data (ICDD) database (2005).

3.3. Thermal analysis

The thermal properties of various types of glasses, specifically the glass transition (T_g) (measured at the midpoint), onset of crystallisation (T_x), crystallisation peak (T_c), melting peak (T_m) temperatures and glass stability against crystallisation (i.e. $\Delta T = T_x - T_g$), were characterised using a simultaneous thermal analysis instrument (SDT, TA Instruments SDT Q600, USA). Approximately 20 mg of glass powder (125–200 μm) was placed into a platinum (for phosphate) or alumina (for silicate) pan and then heated from room temperature to up to 1300 °C at 20 °C min^{-1} heating rate, under 100 mL min^{-1} of nitrogen gas flow. An empty pan was also analysed to determine the baseline which was then subtracted from the thermal traces using TA Universal Analysis 2000 software.

Table 2
Compositional analysis for six different types of glass formulations via EDX analysis.

Components (mol %)	Glass formulations					
	P40	45S5 Expected/ Actual	45S5 + 2 mol% Borax Expected/Actual	45S5 + 5 mol% Borax Expected/Actual	45S5 + 2 mol% V_2O_5 Expected/Actual	45S5 + 5 mol% V_2O_5 Expected/Actual
SiO_2	–	46.1/47.5 ± 0.5	46.1/-	46.1/-	46.1/45.2 ± 1.4	46.1/44.1 ± 1.3
P_2O_5	40/39.9 ± 0.1	2.6/3.1 ± 0.2	2.6/-	2.6/-	2.6/2.6 ± 0.3	2.6/2.7 ± 0.2
MgO	24/23.5 ± 1.7	–	–	–	–	–
CaO	16/16.3 ± 1.6	26.9/26.5 ± 1.2	26.9/-	26.9/-	26.9/27.5 ± 0.9	26.9/27.3 ± 1.1
Na_2O	20/20.3 ± 0.6	24.4/22.9 ± 1.3	22.4/-	19.4/-	22.4/23.1 ± 1.2	19.4/20.9 ± 0.9
Borax	–	–	2/-	5/-	–	–
V_2O_5	–	–	–	–	2/1.7 ± 0.2	5/5.1 ± 0.2

These measurements were made in triplicate.

3.4. Viscosity measurements

Viscosity of the glasses were measured using a high temperature rotational viscometer (Theta industries Rheotronic II 1600 °C Rotating Viscometer, Brookfield DV-III UTRA, USA). The viscosity was determined by measuring the shear stress and the shear rate exerted by the viscous fluid on a rotating cylindrical platinum spindle according to:

$$\eta = \frac{\tau}{\gamma} \tag{1}$$

where, η is the viscosity in poise, τ is the shear stress in dynes/cm^2 and γ is the rate of shear in sec^{-1}.

In order to derive a viscosity curve for glasses, the fixed viscosity at glass transition temperature [20] and the viscosity data obtained via rotational method were used and fitted to the Vogel–Fulcher–Tammann (VFT) Equation 2 [21] by a least squares calculation [22]. The equation is:

$$Log(\eta) = A + B/(T - T_o) \tag{2}$$

where, T is the temperature in °C, η is the viscosity in Pas and *A, B* and T_o are constants.

Viscosity of the glasses was also measured via Hot Stage Microscopy (HSM) analysis which provided information on the temperatures for various characteristic points (i.e. first shrinkage, maximum shrinkage, sphere, hemisphere and flow point/melt temperature) which is described in further detail in the results section. A cylinder-shaped sample with an estimated diameter of ~ 2 mm and the sample height of around 3 mm was used for HSM analysis. The instrument used was a Misura 3 HSM 1400–50 at a heating rate of 5 °C/min for all HSM measurements.

4. Results

4.1. Initial trials to prepare bio-silicate glass microspheres using flame spheroidisation method

Initial invmeasurements..to prepare porous bioactive silicate glass microspheres were explored using similar parameters used to make porous phosphate and borate glass microspheres (i.e. particle to porogen
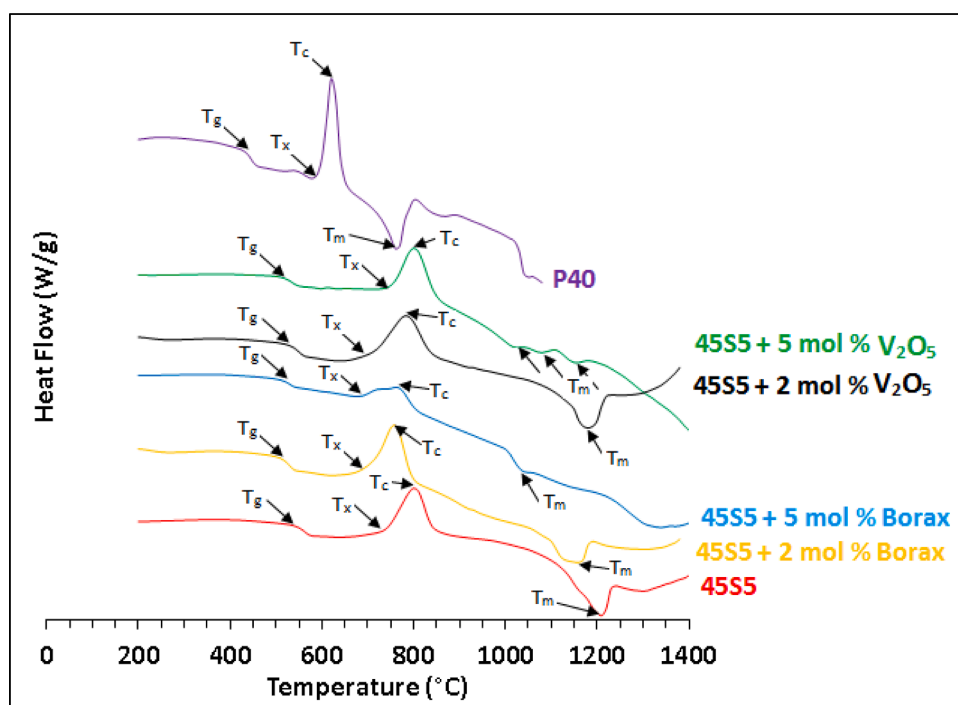

Fig. 2. DSC curves for the six different glass formulations investigated at 20 °C min^{-1} heating rate. T_g = glass transition, T_c = crystallisation peak and T_m = melting temperature.
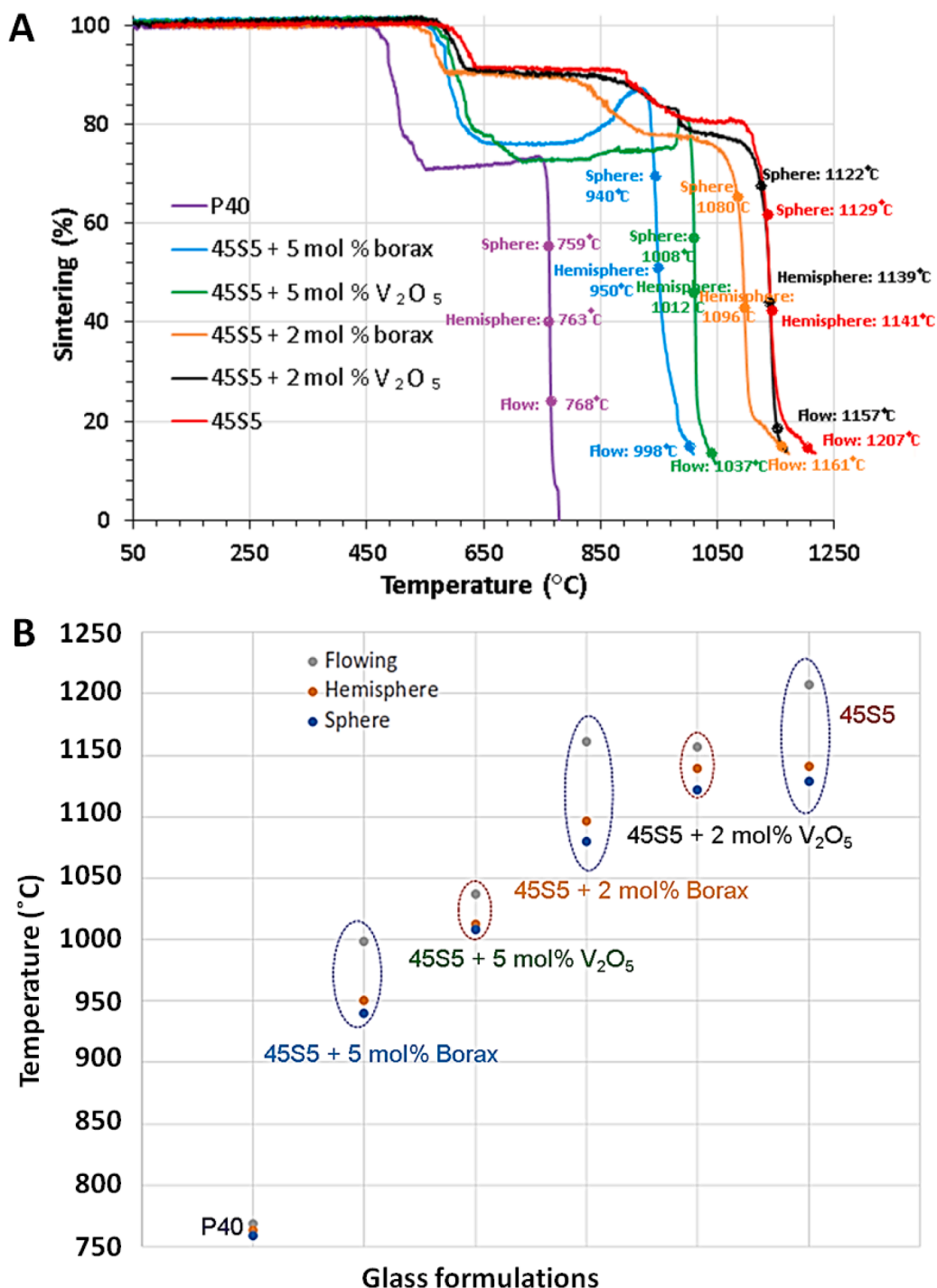
Fig. 3. A) Percentage of sintering as a function of temperature for the different glass formulations investigated via Hot Stage Microscopy (HSM). B) Temperature difference amongst flow, hemisphere and sphere point for the glass formulations investigated via Hot Stage Microscopy (HSM).

(CaCO$_3$) ratio (1:3) and gas flow rate (2.5:2.5) [2]. Our 'conventional' method utilises ground glass particles mixed with porogen directly and the outcomes are presented in Figs. 1A) 45S5 B) S53P4 and C) 13–93. However, although a good production yield of spherical particles was obtained, it was observed that the porosity features and quantity of porous microspheres were very low. We then explored use of SrCO$_3$ as the porogen materials due to its higher decomposition temperature of 1100–1200 °C, which was closer to the melt profiles of the bioactive silicate glasses (1200–1250 °C), as compared to CaCO$_3$ (~800 °C). 13–93 bio-silicate glass was investigated further with different ratios (i. e. 1:3, 1:4 and 1:5) of glass particles to porogen (SrCO$_3$) and the

outcomes are presented in Figs. 1D-F. However, unsatisfactory results (in terms of porous features, quantity of porous microspheres, sphericity etc.) were obtained from these trials.

Due to initial unsuccessful trials (as shown in Fig. 1), a hypothesis was formulated that altering the viscosity profiles of the glasses would aid the porous microsphere manufacturing process. This was based on the previous success of porous microspheres manufactured from phosphate and borate-based glasses.
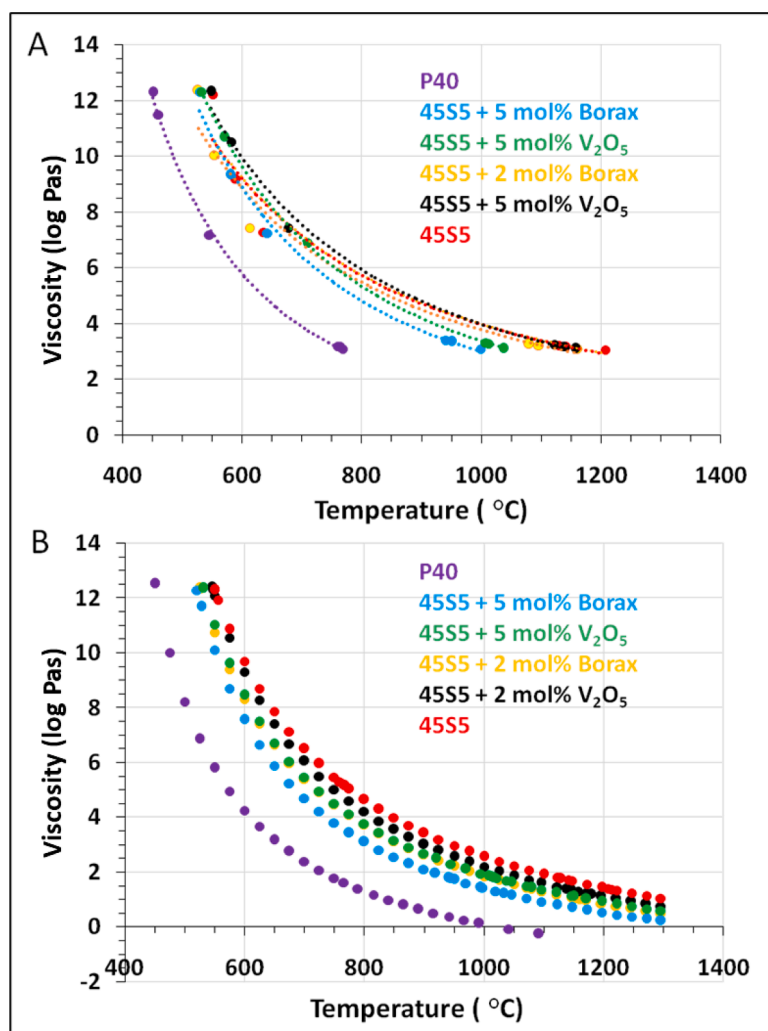
Fig. 4. A) Combined fixed point viscosity curves (fitted) for all six different glass formulations investigated via Hot Stage Microscopy (HSM). B) Fitted viscosity curves for six different glass formulations investigated via high-temperature viscometer.

4.2. Addition of viscosity modifiers: compositional analysis

Borax and V_2O_5 were added to 45S5 glass to explore their effect mainly on viscosity as these are known viscosity modifiers [21,23]. Literature reports show that borax ($Na_2B_4O_7 \cdot 10H_2O$) and V_2O_5 acting as viscosity modifiers can reduce the melting temperature of glass [21,23]. Therefore, 2 and 5 mol% borax and V_2O_5 doped 45S5 glasses were prepared along with 45S5 glass alone for further analysis and microsphere production trials. As previously highlighted, porous microspheres were formed from phosphate glass via our conventional processing method [2], as such the phosphate glass formulation P40 ($40P_2O_5$–$24MgO$–$16CaO$–$20Na_2O$; in mol%) was also included for comparative thermal (i.e. melting) and viscosity analysis with the silicate based glasses (as highlighted in Table 2).

Table 2 shows compositional analysis derived from EDX analyses of the glass formulations produced. Experimental compositional analysis for 45S5 and V_2O_5 containing 45S5 glasses were found to be close to expected composition. Although EDX analysis was also conducted for the borax containing glasses, the results did not show satisfactory data for B, so we have not included it. This is a known issue for EDX analysis and detecting boron as it is very light element.

4.3. Thermal analysis

Fig. 2 shows the thermal profiles of the glasses, where the

corresponding glass transition (T_g), onset of crystallisation (T_x), crystallisation peak (T_c) and melting (T_m) temperature have been labelled. It can be seen from Fig. 2 that the melting temperature for 45S5 (1213 °C) was 450 °C higher in comparison to P40 (766 °C). It was also observed that the thermal properties especially T_g and initial melting (T_m) temperatures for 45S5 glass decreased with increasing borax or V_2O_5 content (see ESI Table 1). For example, the initial melting temperature (T_m) was seen to decrease from 1213 °C (for 45S5) to 1033 °C (for 45S5 + 5 mol% borax) and 1017 °C (for 45S5 + 5 mol% V_2O_5). In addition, three melt peaks were observed for 45S5 + 5 mol% V_2O_5 at 1017 °C, 1075 °C and 1140 °C.

4.4. Viscosity measurement

Viscosity profiles for the glasses were measured indirectly via Hot Stage Microscopy (HSM) analysis and directly via a Searl type high temperature viscometer. HSM analysis provided information on the temperature for five characteristic points as follows: first shrinkage; maximum shrinkage; sphere; hemisphere and flow point/melt temperature. The data obtained enabled plots of the viscosity curves to be compared, including the temperature differences between sphere/hemisphere and flow points, all of which are associated with viscosity changes relative to temperature. The first two temperatures (i.e. first shrinkage, maximum shrinkage) were extracted from the sintering curve profiles and the last three temperatures (i.e. sphere, hemisphere and

Table 3

Rate of viscosity change between two points (i.e. flow and sphere or flow and hemisphere) for six different types of glass formulations investigated via HSM (Hot Stage Microscopy) and HTV (High Temperature Viscometer).

Formulations	Flow-Sphere (slope negative) (log Pas/ °C)		Flow-hemisphere (slope negative) (log Pas/ °C)	
	HSM ($\times 10^{-3}$)	HTV ($\times 10^{-3}$)	HSM ($\times 10^{-3}$)	HTV ($\times 10^{-3}$)
P40	10.09	10.06	10.01	9.97
45S5	2.00	4.74	1.96	4.67
45S5+2 mol% Borax	2.28	4.73	2.22	4.63
45S5+2 mol% V_2O_5	3.79	4.80	3.71	4.70
45S5+5 mol% Borax	5.67	6.46	5.57	6.35
45S5+5 mol% V_2O_5	7.18	6.86	7.14	6.72

flow) were determined based on height, width ratio and contact angle of materials taken from snapshot images using the software supplied with the HSM microscope (see ESI Figure 1).

The three characteristic points (i.e. sphere, hemisphere and flow) were also marked on the sintering curves of each glass composition (see Fig. 3A).

Fig. 3A represents the sintering percentage (i.e. relative height of the sample in%) for the glass compositions investigated against temperature obtained via HSM. It was clearly observed that the sintering profile for the P40 glass (purple line) occurred at the lowest temperature as compared with the 45S5 and borax or V_2O_5 containing 45S5 glass. Moreover, the sintering curves shifted to lower temperature (i.e. towards the P40 sintering curve) with increasing borax or V_2O_5 content in 45S5 glass. The highest shift was observed with addition of 5 mol% borax (blue line) followed by the 5 mol% V_2O_5 (green line), 2 mol% borax (amber line) then 2 mol% V_2O_5 (black line) and finally 45S5 (red line) glass alone.

Fig. 3B represents temperature points for the following three different characteristics i) flow, ii) hemisphere and iii) sphere, for each of the glass compositions investigated. The change from sphere or hemisphere to flow point occurred very rapidly for the P40 phosphate glass compared to 45S5 glass as can be seen from Fig. 3B. Moreover, a smaller spread of these value ranges was observed for the V_2O_5 containing 45S5 glasses in comparison to borax containing 45S5 glasses, which revealed a much larger range between the hemisphere and flow point characteristics.

To further investigate the rate of viscosity change, viscosity vs temperature curves were obtained and plotted using the fixed viscosity for the characteristic temperature points such as flow, hemisphere, sphere, maximum shrinkage and first shrinkage obtained using the HSM analysis [20,24].

The viscosity fitting curves using Vogel-Fulcher-Tammann (VFT) equation were plotted based on the characteristic temperature points obtained via HSM and viscosity at glass transition temperature (as shown in ESI Figure 2). Literature reports the fixed viscosity around $10^{12.3}$ Pa s for glass transition temperature [20]. The six fixed point viscosity characteristics (i.e. flow, hemisphere, sphere, maximum shrinking, first shrinkage and glass transition temperature) were used to fit the viscosity curves using VFT equation (see ESI Figure 2). Fig. 4A represents the fitted viscosity curves for the formulations investigated.

Viscosity can also be measured directly using a high-temperature rotating viscometer, and these viscosity profiles were also obtained for the six glass formulations investigated. ESI Figure 3 represents the viscosity fitting curves for the glass formulations investigated (using VFT equation) based on high temperature viscosity (HTV) data and the fixed viscosity for glass transition point (see fitted viscosity curves in Fig. 4B).

The viscosity curves obtained via HTV followed similar trends to the viscosity curves obtained via HSM. Fig. 4 shows that the viscosity curves

Table 4

Several trials of flame spheroidisation for different glass composition and different process parameters like starting glass particles size, gas flow rate ratio, outcomes based on surface and cross-sectional images.

Compositions	Starting particle size ranges (μm)	Gas flow rate ratio	Outcomes based of surface and cross-sectional images of microspheres	Evidence
45S5 + 2 mol % borax	63–125	3:3	70–80% microspheres were fully porous, and the rest exhibited only surface pores with a large solid core.	Figs. 5A-B
45S5 + 5 mol % borax	63–125	3:3	The microspheres exhibited rough surface textures after washing. Some microspheres only had surface pores with a large solid core, whilst some had large cavities inside and some of the microspheres were full porous	Figs. 5C-D
45S5 + 2 mol % V_2O_5	63–125	3:3	70–80% of the microspheres were fully porous whilst the remainder exhibited only surface pores with solid cores. Larger pores were also observed for 2 mol% V_2O_5 containing 45S5 compared to 2/5 mol% borax containing 45S5.	Figs. 5E-F
45S5 + 5 mol % V_2O_5	63–125	3:3	Highly porous microspheres (>95%) with fully interconnected pores were produced	Figs. 5G-H
45S5	63–125	3:3	Only a few porous microspheres with small pores were observed. Some microspheres were solid (represented with red circles) whilst some microspheres only exhibited surface pores with a solid core (represented with amber circles), and some only had large cavities inside the microspheres (represented with yellow circles). Also, the few microspheres observed which were fully porous, were relatively smaller in size (shown as green circles)	Figs. 6A-B
45S5	63–71	3:3	Highly porous microspheres with large pores were formed. The yield more than 95% microspheres seen with full porosity.	Figs. 6C-D
45S5	63–125	3.5:3.5	More than 90% microspheres were fully porous.	Figs. 7A-B
45S5	63–125	4:4	More than 90% microspheres were fully porous.	Figs. 7C-D
45S5	63–125	4.5:4.5	More than 90% microspheres were fully porous.	Figs. 7E-F

Table 5

Chemical compositions for starting 45S5 bulk glass and 45S5 PGMS (cross-sectional samples) for the different starting particle sizes (i.e. 63–71 μm and 63–125 μm) and gas flow rate ratios (i.e. 3:3, 3.5:3.5, 4:4 and 4.5:4.5) obtained via EDX analysis.

Formulations	SiO_2 (mol%)	P_2O_5 (mol%)	CaO (mol%)	Na_2O (mol%)
45S5-Starting bulk glass	47.5 ± 0.2	3.1 ± 0.1	26.5 ± 0.7	23.0 ± 0.2
45S5-PGMS (63–71 μm, gas flow rate ratio-3:3)	47.7 ± 1.5	2.6 ± 0.1	28.3 ± 0.6	21.4 ± 1.6
45S5-PGMS (63–125 μm, gas flow rate ratio-3.5:3.5)	46.6 ± 1.3	2.7 ± 0.2	28.9 ± 1.9	21.8 ± 0.8
45S5-PGMS (63–125 μm, gas flow rate ratio-4:4)	46.6 ± 1.3	2.7 ± 0.2	27.4 ± 0.4	23.3 ± 0.6
45S5-PGMS (63–125 μm, gas flow rate ratio-4.5:4.5)	46.8 ± 0.5	2.6 ± 0.1	27.7 ± 0.8	22.9 ± 0.5

shifted to lower temperature with increasing borax or V_2O_5 content in 45S5 glass. A higher shift of the viscosity curve was observed for the 5 mol% borax containing 45S5 glass in comparison to 5 mol% V_2O_5 45S5. However, the fittings for the viscosity curves obtained via HTV (ESI Figure 3) were more accurate compared to the viscosity curves obtained via HSM (ESI Figure 2). The rate of viscosity changes (slope) in between melt and hemisphere temperature and/or between melt and sphere temperature for all six glass formulations were calculated from viscosity curves (from both HSM and HTV methods) as presented in Table 3. The slope between melt and sphere temperature was considered a straight line as transformation from melt to spheres occurred very quickly (by lowering 9 °C only for P40 and 78 °C (highest) for 45S5, see Fig. 3). The rate of viscosity change (melt-sphere/melt-hemisphere) was 125% higher for P40 (as observed via HTV) compared to 45S5. The rate of viscosity change (melt-sphere/melt-hemisphere) for 45S5 increased with increasing borax or V_2O_5 in 45S5. For example, a 45% higher rate of viscosity change was observed for the 5 mol% V_2O_5 45S5 glass compared to 45S5 alone. Moreover, a higher rate of viscosity change (melt-sphere/melt-hemisphere) was observed for the V_2O_5 containing 45S5 glass when compared to borax containing 45S5 (see Table 3).

4.5. Influence of gas flow ratios

It was also noticed that the flame length could be changed by varying the gas flow rate ratios. To confirm this the flame lengths were measured to investigate their variation with gas flow ratio and are shown in ESI Figure 4. The flame length decreased from approximately 37 cm to 31 cm with increasing gas flow rate ratio from 2:2 to 3:3. As such, adjusting the gas pressures, which altered the flame lengths, could also influence the particle residence time within the flame and thereby subsequently effect the cooling rate of the particles. For example, particles exiting the shorter flame, had reduced particle residence time and faster cooling rate.

4.6. Flame spheroidisation trials

As the melt temperature and viscosity for 45S5 glass decreased significantly with the addition of borax or V_2O_5, further trials of spheroidisation for both the 2 and 5 mol% borax and V_2O_5 45S5 and 45S5 alone were conducted using the same parameters as the initials trials (i.e. starting glass particle size range, particles to porogen ratio, porogen size range etc.) with the exception of gas flow rate ratios. The gas flow rate ratio of 3:3 was trialled instead of 2.5:2.5 (used in the initial trial) to explore if increasing cooling rate for molten microparticles would be beneficial. Moreover, trials for the 45S5 glass alone were also conducted focussing on use of smaller starting size range particles (i.e. between 63 and 71 μm) and with varying gas flow rate ratios (i.e. 3.5:3.5, 4:4, 4.5:4.5) to further increase their cooling rate. Outcomes for these trials are presented in Table 4 below.

4.7. XRD of porous 45S5 glass microsphere

To explore whether the materials produced remained amorphous, XRD analysis was conducted and presented in Fig. 8. A small sharp peak was observed for the PGMS profiles which was matched to $CaCO_3$ used as the porogen material for manufacturing the PGMS. This suggested that some residual porogen material remained in the pores of these microspheres, even after the wash-step.

4.8. Compositional analysis of porous 45S5 glass microsphere

Chemical compositions (mol%) for starting bulk glass and PGMS (cross-sectional samples) from different starting particle size ranges (i.e. 63–71 μm and 63–125 μm) and different gas flow rate ratios (i.e. 3:3, 3.5:3.5, 4:4 and 4.5:4.5) obtained via EDX analysis are presented in Table 5. It was seen that around 2 mol% CaO content increased as compared to starting bulk glass which most likely resulted from decomposition of the porogen materials.

5. Discussion

Food and Drug Administration (FDA) approved bioactive 45S5 and S53P4 glasses are well known and have successfully been used clinically as bone regeneration materials due to their ability to bond to bone tissue [19]. However, these materials have been implemented as irregular-shaped particles which limits their applicability. Developing a rapid cost-effective process to produce spherical and especially porous particles will enable alternate applications to be explored especially with a view towards orthobiologics.

This paper set out to explore the processing parameters of a flame spheroidisation process to demonstrate successful production of PGMS from bioactive silicate glasses. The results revealed that initial attempts to manufacture porous bioactive silicate glass microspheres using our 'Conventional method', following the same parameters (i.e. glass particle to porogen ratio, gas flow rate ratio) used for making porous microspheres from phosphate and borate glasses [1,15] were unsuccessful. These initial unsuccessful attempts were suggested to be due to the large differences between glass melt temperatures (i.e. 1200–1250 °C) and the decomposition temperature of the $CaCO_3$ porogen (~800 °C). The hypothesis here was that if the porogen decomposed earlier than the glass particles had time to melt, then this could impact the pore formation process. Therefore, $CaCO_3$ porogen was substituted with $SrCO_3$, which has a decomposition temperature (1100–1200 °C) closer to the melt profiles of the bioactive silicate glasses. These initial trials using $SrCO_3$ also proved unsatisfactory (in terms of pore features, quantity of porous microspheres, sphericity etc.). These outcomes then led to reconsideration of the higher melt temperatures of these bioactive silicate glasses alongside their viscosity profiles and comparing them to the success achieved with phosphate glasses, which formed highly porous microspheres [2]. Therefore, 2 and 5 mol% borax and V_2O_5 were added to biosilicate glass 45S5 to alter its thermal and viscosity profiles.

The melt (T_m) temperatures for 45S5 glass decreased by approximately 200 °C with the addition of 5 mol% borax or V_2O_5 in place of Na_2O in 45S5 (see ESI Table 1). This was attributed to the lower melting temperature for borax (450–510 °C) and V_2O_5 (690 °C) compared to Na_2O (1132 °C). Wang *et.al.* studied the effect of B_2O_3 on melting temperature, viscosity and desulfurisation capacity of CaO–based refining flux and reported that the low melting temperature of B_2O_3 (~450 °C), was favourable for decreasing the melt temperature of higher melting temperature components such as CaO and Al_2O_3 [25]. Moreover, they reported that the viscosity for (CaO)(60%)–(Al_2O_3)(20%)–MgO(8%)–SiO_2(8%) decreased significantly with addition of 4 mass% B_2O_3 compared to the equal mass% of CaF_2 [25].

Viscosity is an important property in glass making and is dependant on the chemical glass composition as well as temperature. The viscosity must be tightly controlled during glass forming processes to maintain a
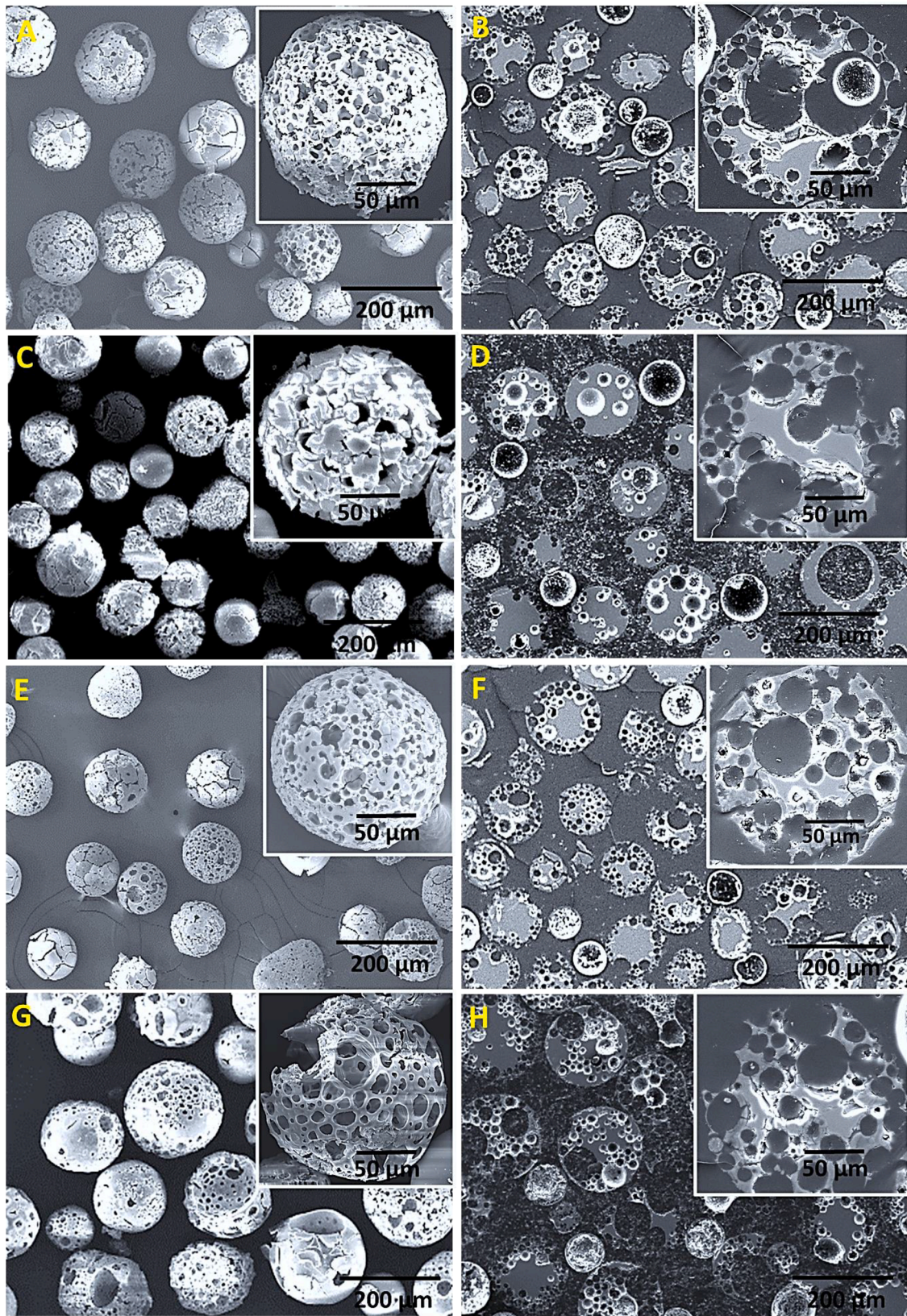
Fig. 5. SEM images of washed and cross-sections of A-B) 45S5 + **2 mol% borax,** C-D) 45S5 + **5 mol% Borax**, E-F) 45S5 + **2 mol% V$_2$O$_5$** and G-H) 45S5 + **5 mol% V$_2$O$_5$** microspheres.
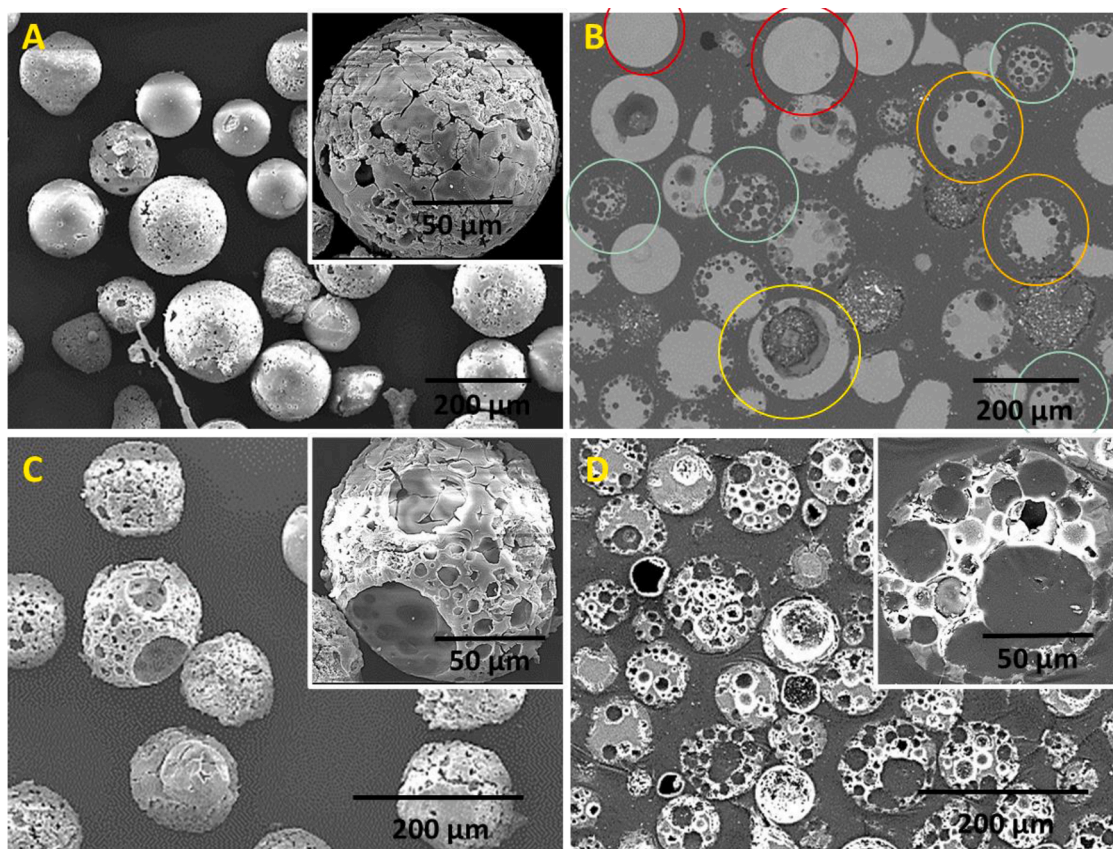
Fig. 6. SEM images of washed and cross-sections of A-B) 45S5 microspheres using 3:3 gas flow rate ratio for 63–125 μm starting glass particles and C-D) 45S5 microspheres using 3:3 gas flow rate ratio for starting glass particles ranging between 63 and 71 μm.

high-quality product and temperatures throughout the glass cooling schedule are also dictated by the viscosity.

In this study viscosity for the glasses was measured indirectly via Hot Stage Microscopy (HSM) and then directly via rotating cylinder high temperature viscometer (HTV) method. The viscosity fitting curves for the six glass formulations were investigated using the VFT equation (see ESI Figures 2 and 3) and the profiles obtained followed similar trends for both methods (HSM, HTV), where viscosity curves shifted to lower temperatures with the addition of the viscosity modifiers (borax, V_2O_5). This was attributed to the higher oxidation state of B (+3) and V (+5, +4, +3, +2) which generally reduce the viscosity compared to oxidation state Na (+) [26].The viscosity curve for P40 glass had the lowest temperature compared to 45S5 and the borax or V_2O_5 containing 45S5 glasses (see Fig. 4).

The phosphate P40 glass formed excellent quality and high production yield porous microspheres [2] whereas via conventional method utilising similar processing parameters, 45S5 did not (see Fig. 1A). However, after addition of viscosity modifiers, both borax and V_2O_5 containing 45S5 glass formed porous microspheres although slightly higher gas flow rate ratio of 3:3 was used instead of 2.5:2.5. It was interesting to note that the 5 mol% V_2O_5 containing 45S5 glass formed highly porous microspheres compared to the 5 mol% borax containing 45S5 glass (see cross-section, Figs. 5D and H), which was unexpected based on the viscosity results showing that the borax formulation had significantly lower viscosity compared to the V_2O_5 formulation, although both had very similar melt temperatures.

These results were then correlated with the HTM profiles to explore the temperature differences between flow and hemisphere/sphere point (see Fig. 3B), which also related to viscosity change relative to temperature. Here we observed there was a much smaller temperature gap between flow and hemisphere/sphere point for the 5 mol% V_2O_5

containing 45S5 in comparison to 5 mol% borax containing 45S5. Moreover, it was also noted that the viscosity changes relative to temperature between flow and sphere or hemisphere point occurred rapidly for P40 compared to 45S5 glass (see from Fig. 3B). These results also corelated to the rate of viscosity change between flow and hemisphere/sphere points from fitting viscosity curves obtained via HSM and HTM (see Table 3). Therefore, in our flame spheroidisation process we propose that the rate of change in viscosity is a highly influential and important factor to successfully producing desirable porous microspheres. We also observed that the flame length can be altered with gas flow rate ratio which could also influence particle residence time within the flame as well as the cooling rate of the particles ejected from the flame. According to reports in the literature, the temperature of the oxyacetylene flame can range between 3100 and 3300 °C [27,28]. However, the experimental flame temperature may vary with variation of gas flow rate ratios as well as from introduction of varying material particles for processing. As part of a follow-up study, we are looking to explore and model the flame temperature at varying ratios as well as the influence of introducing different materials using appropriate thermal analysis cameras.

From the outcomes and observations above, a processing model has been assembled taking into consideration factors which could influence the success of manufacturing porous microspheres as presented in Fig. 9 below.

It's also worth noting that although the flame spheroidisation process developed to convert irregular shaped particles into porous microspheres takes less than a second (i.e. in milliseconds), there are many parameters involved to achieve the desired outcome, as highlighted in Fig. 9.

Furthermore, the rate of viscosity change can also be influenced by increasing cooling rate as a result of increasing gas flow rate ratio and
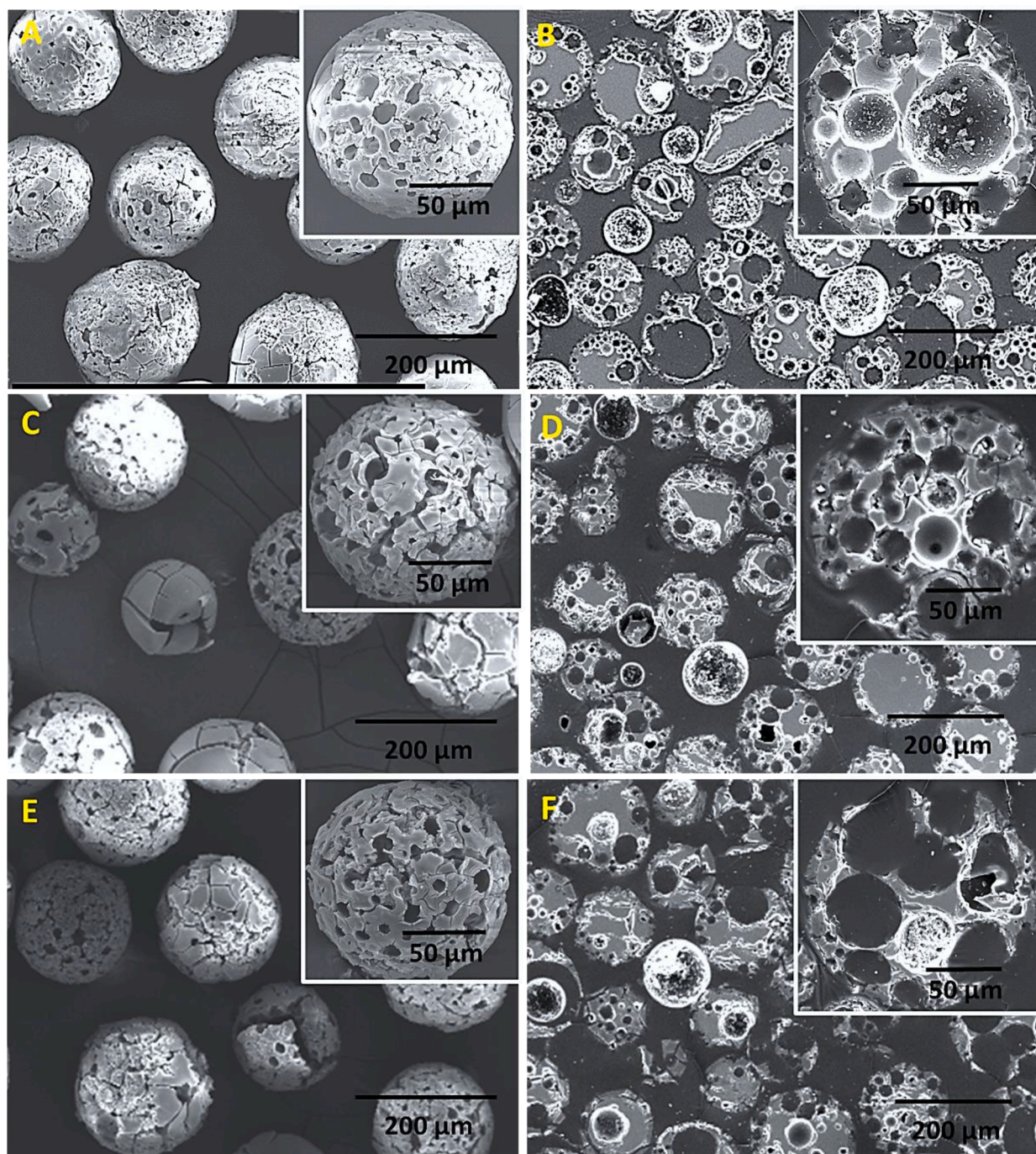
Fig. 7. SEM images and cross-sections for porous 45S5 microspheres (washed) using A-B) 3.5:3.5, C-D) 4:4 and E-F) 4.5:4.5 gas flow rate ratio for starting glass particles ranging between 63 and 125 μm.

this result reflected on the trial for producing borax containing 45S5 and 45S5 glass alone using 3:3 gas flow rate ratio instead of 2.5:2.5 as used in the initial trials. It was observed that partially porous 45S5 microspheres were formed when using 3:3 gas flow rate ratio, whereas some microspheres were solid (as shown in red circles) and other microspheres only exhibited surface pores with a solid core (represented as amber circles). Some microspheres only presented with a large cavity inside the microspheres (shown in yellow circles) and a few microspheres were fully porous (shown in green circles, see cross-sections, Fig. 6B). For the microspheres with large cavity inside, two possibilities may be responsible; 1) Smaller gas bubbles may have coalesced together to form larger gas bubbles inside the microspheres, or 2) Larger

porogen or large quantity of porogen had become entrapped inside the molten glass during spheroidisation leading to large gas volume within the microspheres. For the microspheres observed only with surface pores and a large solid core, two possibilities may have contributed; 1) Glass particles may not have fully melted and therefore, the porogen had penetrated only the surface of microsphere as 45S5 glass had higher melting temperature and viscosity. Or 2) Gas bubbles produced within the molten glass may have moved towards the surface as the rate of viscosity change for 45S5 or 5 mol% borax containing 45S5 glass was comparatively lower compared to P40 or 5 mol% V_2O_5 containing 45S5 (see Table 3). On the other hand, from the few microspheres which had formed into fully porous microspheres, these were relatively smaller in
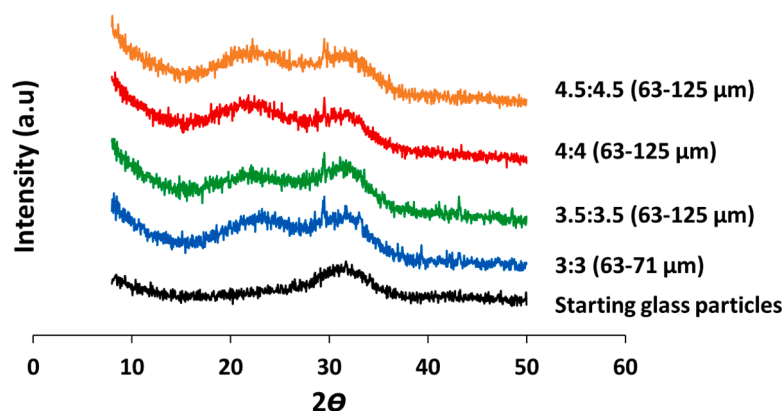
Fig. 8. X-ray diffraction pattern for 45S5 glass (starting particles) and porous 45S5 glass microspheres for different starting particle size (i.e. 63–71 μm and 63–125 μm) and different gas flow rate ratios (i.e. 3:3, 3.5:3.5, 4:4 and 4.5:4.5).
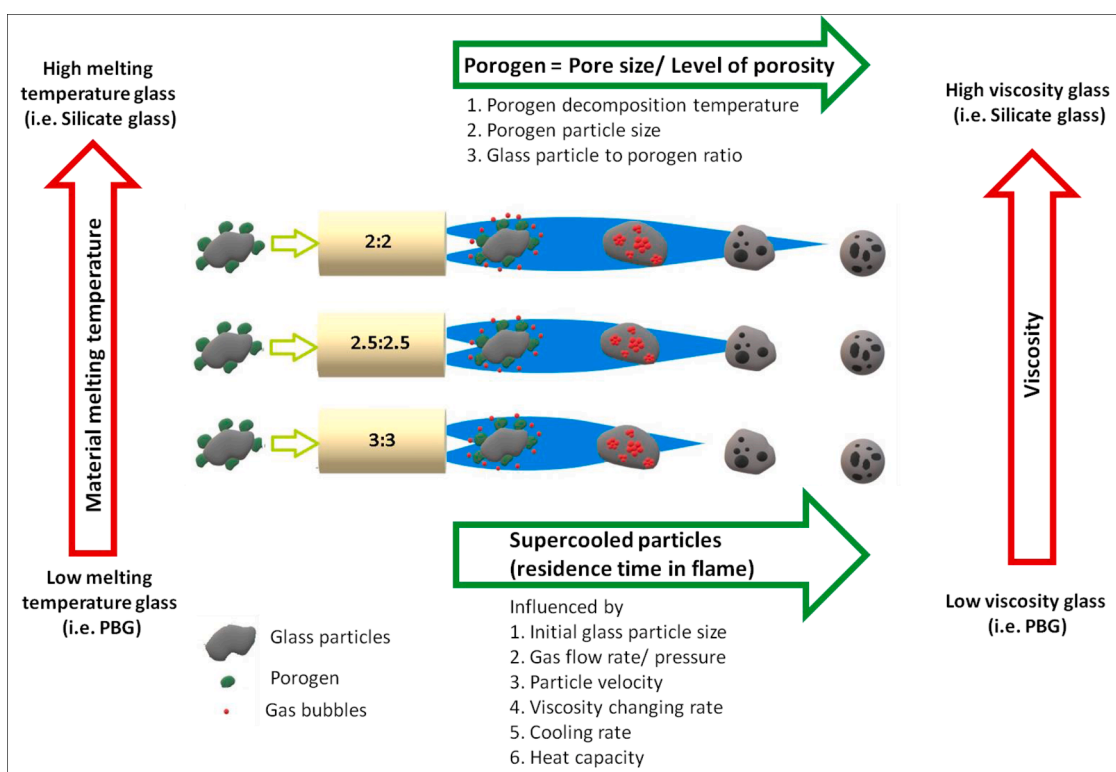

Fig. 9. Proposed model highlighting key parameters which can influence successful production of porous glass microspheres via flame spheroidisation process.

size as compared to the others. As such, subsequent highly porous microspheres of '45S5 glass alone' were successfully produced by choosing both smaller staring particle size ranges (as confirmed via SEM – see Figs. 6C-D) and increasing the gas flow rate ratio thereby increasing cooling rate (of molten glass during exiting the microspheres from the flame, which resulted in the better formation of the pores in the microspheres) for this rapid changing viscosity profile glass (see Fig. 7). Moreover, the PGMS prepared via this flame spheroidisation route retained their amorphous nature (with the exception of a small peak of CaCO₃ observed which was used as porogen) and no significant change in chemical composition had occurred compared to the starting materials. Therefore, by selecting appropriate parameters, this manufacturing process could also be used for other bioactive silicate glasses (i.e. S53P4, 13–93), inorganic materials, such as glass-ceramics (e.g. AW) and metal oxides to develop them as porous materials. For example, successful manufacture of S53P4 porous glass microspheres

using higher gas flow rate ratio (4:4) were also achieved and are shown in ESI Figure 5.

In summary, porous 45S5 microspheres were produced via flame spheroidisation process by choosing the appropriate process parameters (e.g. smaller glass particles or higher gas flow rate ratio which increased the cooling rate and the rate of viscosity change for the particles exiting the flame).

6. Conclusions

The influence of various process parameters to manufacture of highly porous microspheres utilising flame spheroidisation technique has been summarised in this paper. Attempts to manufacture porous bioactive silicate glass microspheres following the same parameters used for making porous microspheres from phosphate and borate glasses were unsuccessful due to the higher melting temperature (~450 °C) and

higher viscosity of silica. Significant reduction of melt temperature ($\sim$200 °C) and viscosity was observed by the addition of viscosity modifiers (i.e. 5 mol% of borax or V_2O_5), which facilitated successful production of silicate glass microspheres. The viscosity change relative to temperature was determined to be an important factor in the process, in addition to the melt temperature and viscosity profile. Higher yield and highly porous pure 45S5 microspheres were also achieved by manipulating the flame properties (i.e. using higher gas flow rate ratios) which influenced the particle residence times and cooling rates for the molten glass upon exiting the flame. Considering all of the influential parameters, a model for the successful production of porous silica-based glass microspheres via flame spheroidisation has been presented in this paper.

Author contributions

IA contributed to conception. IA, MTI contributed to design of the study. JB suggested to add viscosity modifiers. IA provided resources and supervision. MTI and HR carried out experimental work. MTI wrote the first draft of the manuscript. All authors contributed to manuscript revision, read, and approved the submitted version.

Data and code availability

The original contributions presented in the study are included in the article/Supplementary Material, further inquiries can be directed to the corresponding author.

Electronic supplementary information

Snapshot images obtained by Hot Stage Microscopy (HSM) (ESI Figure 1); Viscosity fitting curves using a fixed-point viscosity method via HSM (ESI Figure 2); Viscosity fitting curves investigated via high temperature viscometer (ESI Figure 3); Flame lengths (ESI Figure 4), SEM of S53P4 PGMS (ESI Figure 5); Thermal data (ESI Table 1) (PDF).

Ethical approval

Not applicable.

Declaration of Competing Interest

The authors declare that they have no known competing financial interests or personal relationships that could have appeared to influence the work reported in this paper.

Data availability

Data will be made available on request.

Acknowledgments

Supplementary materials

Supplementary material associated with this article can be found, in the online version, at doi:10.1016/j.jnoncrysol.2023.122393.

References

[1] A. Matamoros-Veloza, et al., Formulating injectable pastes of porous calcium phosphate glass microspheres for bone regeneration applications, J. Mech. Behav. Biomed. Mater. 102 (2020), 103489.

[2] K.M.Z. Hossain, et al., Porous calcium phosphate glass microspheres for orthobiologic applications, Acta Biomater. 72 (2018) 396–406.

[3] S.-.W. Choi, et al., Biodegradable porous beads and their potential applications in regenerative medicine, J. Mater. Chem. 22 (23) (2012) 11442–11451.

[4] Y. Cai, et al., Porous microsphere and its applications, Int. J. Nanomed. 8 (2013) 1111.

[5] J.S. McLaren, et al., Porous Phosphate-Based Glass Microspheres Show Biocompatibility, Tissue Infiltration, and Osteogenic Onset in an Ovine Bone Defect Model, ACS Appl. Mater. Interfaces 11 (17) (2019) 15436–15446.

[6] V. Karageorgiou, D. Kaplan, Porosity of 3D biomaterial scaffolds and osteogenesis, Biomaterials 26 (27) (2005) 5474–5491.

[7] B.-.S. Chang, et al., Osteoconduction at porous hydroxyapatite with various pore configurations, Biomaterials 21 (12) (2000) 1291–1298.

[8] O. Gauthier, et al., Macroporous biphasic calcium phosphate ceramics: influence of macropore diameter and macroporosity percentage on bone ingrowth, Biomaterials 19 (1–3) (1998) 133–139.

[9] J. Diao, et al., 3D-Plotted Beta-Tricalcium Phosphate Scaffolds with Smaller Pore Sizes Improve In Vivo Bone Regeneration and Biomechanical Properties in a Critical-Sized Calvarial Defect Rat Model, Adv Healthc Mater 7 (17) (2018), 1800441.

[10] K.M.Z. Hossain, U. Patel, I. Ahmed, Development of microspheres for biomedical applications: a review, Prog Biomater 4 (1) (2015) 1–19.

[11] N.J. Lakhkar, et al., Titanium phosphate glass microspheres for bone tissue engineering, Acta Biomater. 8 (11) (2012) 4181–4190.

[12] J. Martinelli, et al., Synthesis and characterization of glass–ceramic microspheres for thermotherapy, J. Non. Cryst. Solids 356 (44–49) (2010) 2683–2688.

[13] S.D. Conzone, et al., *In vitro and in vivo dissolution behavior of a dysprosium lithium borate glass designed for the radiation synovectomy treatment of rheumatoid arthritis*, Journal of Biomedical Materials Research: An Official Journal of The Society for Biomaterials 60 (2) (2002) 260–268.

[14] H. Fu, M.N. Rahaman, D.E. Day, Effect of process variables on the microstructure of hollow hydroxyapatite microspheres prepared by a glass conversion method, J. Am. Ceram. Soc. 93 (10) (2010) 3116–3123.

[15] M.T. Islam, et al., Rapid conversion of highly porous borate glass microspheres into hydroxyapatite, Biomater. Sci. 9 (5) (2021) 1826–1844.

[16] S. Li, et al., Porous-wall hollow glass microspheres as novel potential nanocarriers for biomedical applications, Nanomed. Nanotechnol. Biol. Med. 6 (1) (2010) 127–136.

[17] W. Hong, et al., A hierarchically porous bioactive glass-ceramic microsphere with enhanced bioactivity for bone tissue engineering, Ceram. Int. 45 (10) (2019) 13579–13583.

[18] J. Kraxner, et al., Porous bioactive glass microspheres prepared by flame synthesis process, Mater. Lett. 256 (2019), 126625.

[19] M.T. Islam, et al., Evolution of silicate bioglass particles as porous microspheres with a view towards orthobiologics, J. Biomater. Appl. 36 (8) (2022) 1427–1443.

[20] M. Garcia-Valles, et al., Calculation of viscosity–temperature curves for glass obtained from four wastewater treatment plants in Egypt, J. Therm. Anal. Calorim. 111 (1) (2013) 107–114.

[21] A. Fluegel, Glass viscosity calculation based on a global statistical modelling approach, Glass Technol.-Eur. J. Glass Sci. Technol. Part A 48 (1) (2007) 13–30.

[22] L. Koudelka, P. Mošner, Study of the structure and properties of Pb–Zn borophosphate glasses, J. Non. Cryst. Solids 293 (2001) 635–641.

[23] F.V. Tooley, The Handbook of Glass manufacture: a Book of Reference For the Plant executive, technologist, and Engineer, Ogden Publishing Company, New York, 1953.

[24] F. Montanari, et al., Calibration and use of the heating microscope for indirect evaluation of the viscosity and meltability of archeological glasses, Int. J. Appl. Glass Sci. 5 (2) (2014) 161–177.

[25] H. Wang, et al., Effect of B_2O_3 on melting temperature, viscosity and desulfurization capacity of CaO–based refining flux, ISIJ Int. 51 (5) (2011) 702–706.

[26] P. Hewlett, L. Martin. *Lea's chemistry of cement and concrete*, Butterworth-Heinemann, United Kingdom,, 2019.

[27] T.L. Brown, et al.. Chemistry: the Central Science, Pearson Education, United Kingdom, 2002.

[28] A.Z. Lua'y, P.W. Morrison, Optimizing diamond growth for an atmospheric oxyacetylene torch, J. Mater. Res. 12 (5) (1997) 1237–1252.